Open Access

The retinal pigment epithelium displays electrical excitability and lateral signal spreading

Irina Ignatova[1], Roman Frolov[2] and Soile Nymark[1*]

Abstract

Background The non-neuronal retinal pigment epithelium (RPE) functions in intimate association with retinal photoreceptors, performing a multitude of tasks critical for maintaining retinal homeostasis and collaborating with retinal glial cells to provide metabolic support and ionic buffering. Accordingly, the RPE has recently been shown to display dynamic properties mediated by an array of ion channels usually more characteristic of astrocytes and excitable cells. The recent discovery of canonical voltage-activated Na^+ channels in the RPE and their importance for phagocytosis of photoreceptor outer segments raises a question about their electrogenic function. Here, we performed a detailed electrophysiological analysis related to the functioning of these channels in human embryonic stem cell (hESC)-derived RPE.

Results Our studies examining the electrical properties of the hESC-RPE revealed that its membrane mainly displays passive properties in a broad voltage range, with the exception of depolarization-induced spikes caused by voltage-activated Na^+ current (I_{Na}). Spike amplitude depended on the availability of I_{Na} and spike kinetics on the membrane time constant, and the spikes could be largely suppressed by TTX. Membrane resistance fluctuated rapidly and strongly, repeatedly changing over the course of recordings and causing closely correlated fluctuations in resting membrane potential. In a minority of cells, we found delayed secondary I_{Na}-like inward currents characterized by comparatively small amplitudes and slow kinetics, which produced secondary depolarizing spikes. Up to three consecutive delayed inward current waves were detected. These currents could be rapidly and reversibly augmented by applying L-type Ca^{2+} channel blocker nifedipine to diminish influx of calcium and thus increase gap junctional conductance.

Conclusions This work shows, for the first time, that I_{Na} and I_{Na}-mediated voltage spikes can spread laterally through gap junctions in the monolayer of cells that are traditionally considered non-excitable. Our findings support a potential role of the RPE that goes beyond giving homeostatic support to the retina.

Keywords RPE, Electrical excitability, Spikes, Ion channels, Patch clamp

*Correspondence:
Soile Nymark
soile.nymark@tuni.fi
[1] Faculty of Medicine and Health Technology, Tampere University, Tampere, Finland
[2] Independent Researcher, Oulu, Finland

Ignatova *et al. BMC Biology*   (2023) 21:84

Page 2 of 19

Background

Retinal pigment epithelium (RPE) is adjacent to photo-receptors in the eye and critical for normal retinal functioning. RPE secretes growth factors; phagocytoses the exhausted fragments of photoreceptor outer segments (POS); regenerates the visual pigment; maintains ionic homeostasis of the sub-retinal space by transporting ions, water, and metabolic end products between the sub-retinal space and the blood; serves as a barrier between the bloodstream and the retina; absorbs light; and protects the retina from photo-oxidation [1, 2]. A loss or failure of any RPE function can have pathologic consequences in the retinal tissue leading to photoreceptor degeneration and even blindness [2, 3]. Several of these functions depend on ion channels expressed in the plasma membrane [2, 4–10] .

The channelome of RPE is large and includes many ligand- and voltage-activated channels with functional verification to at least TRP (TRPC1, 4; TRPV2); inwardly (Kir4.1, 6.2, 7.1) and outwardly rectifying voltage-activated K^+ channels (K_V1.2, 1.3, 1.4, 4.2; KCNQ1, 4, 5); Ca^{2+}-activated K^+ channels (BK); voltage-activated Ca^{2+} channels (Ca_V1.2, Ca_V1.3, Ca_V3.1, Ca_V3.2); Cl^- channels (ClC-2, best-1, cystic fibrosis transmembrane conductance regulator (CFTR)); connexin channels; and voltage-gated Na^+ channels [5–8, 11–18]. Yet, RPE cells are not neurons; they are traditionally considered to have passive intrinsic properties, similarly to other non-excitable cells. Is this large channelome with several voltage-activated channels present in the RPE only to support its homeostatic activity?

This study was motivated by the question raised above as well as the recent discovery of voltage-activated Na^+ channels in the RPE and their prominent role in the phagocytosis of POS [4]. Immunolabeling and mass spectrometry experiments revealed the expression of nine alpha-subunits of voltage-activated Na^+ channels (Na_V1.1, Na_V1.3 to Na_V1.9, and Na_X), especially Na_V1.4, Na_V1.6, and Na_V1.8 [4]. It was shown that exposure of RPE to tetrodotoxin (TTX) both in culture and ex vivo in the mouse, and also silencing the expression of Na_V1.4 with shRNA, can suppress phagocytosis, raising a possibility that electrogenic function of these channels might contribute to phagocytosis [4]. By demonstrating the presence of Na^+ channels also in the mouse RPE, these results contradict conclusions of earlier studies, in which inward Na^+ current (I_{Na}) was observed but attributed to the neuronal trans-differentiation of cultured primary RPE [16, 19].

Fast depolarizing voltage responses ("spikes") mediated by I_{Na} have been previously described in the conventional non-excitable cells, including astrocytes and rabbit pigmented ciliary body epithelial cells [20–23].

In the study of cultured neonatal rat RPE, Botchkin and Matthews reported action potential-like depolarizing spikes [16]. However, although many studies have analyzed ionic currents in various RPE cells, our understanding of membrane properties and voltage responses is still incomplete.

Development of functionally mature human embryonic stem cell-derived RPE (hESC-RPE) holds promise for prospective transplantation treatments of RPE-dependent retinal degenerative diseases [24–26]. The hESC-RPE cell lines express RPE-specific genes and proteins, exhibit a hexagonal cobblestone morphology with appropriate polarization and barrier properties, strong pigmentation, and perform phagocytosis similarly to human fetal RPE [5, 27–30]. This functionality and promising outlook of hESC-RPE transplantation necessitate comprehensive study of their electrophysiological properties. In this study, by using the patch-clamp technique, we investigated membrane response properties of hESC-RPE cells in the monolayer in physiological conditions at body temperature. We describe the properties of spikes, a spontaneously and rapidly fluctuating leak conductance, and a previously unreported phenomenon of multiple waves of inward currents caused by signal spreading via gap junctions.

Results

Ionic currents in hESC-RPE

We studied electrophysiological properties of pigmented, cobblestone hESC-RPE cells (Fig. 1A) in whole-cell patch-clamp experiments by recording from 707 cells in voltage clamp mode; in 181 of these cells, additional current-clamp measurements were performed. There was a substantial variability in the ionic currents between cells (Fig. 1C,D). I_{Na} of variable amplitude (see I_{Na} in Fig. 1C and D for comparison) was detected in the majority (~98%) of cells using the recording protocol shown in Fig. 1B. The transient (I_A) and sustained (delayed rectifier, I_{DR}) voltage-activated K^+ currents were expressed at dissimilar ratios (Fig. 1C, D). Similarly, leak conductance varied from cell to cell. Sustained hyperpolarization-activated inward current (I_{IR}, Fig. 1E), possibly mediated by K^+ inward rectifier channels, was found in the majority (~80%) of cells (Fig. 1D) [6].

The ultra-fast transient depolarizing I_{Na} is conducted by several Na^+ channel types [4]. Figure 2 describes the essential aspects of I_{Na} in hESC-RPE at the physiological temperature of 33–35°C. A typical I_{Na} is shown in Fig. 2A. Its amplitude was determined by subtracting the current after the end of the preceding capacitive current (I_C) from the negative peak amplitude. At positive voltages, precise measurement of I_{Na} was often complicated due to progressive superposition of the partly compensated
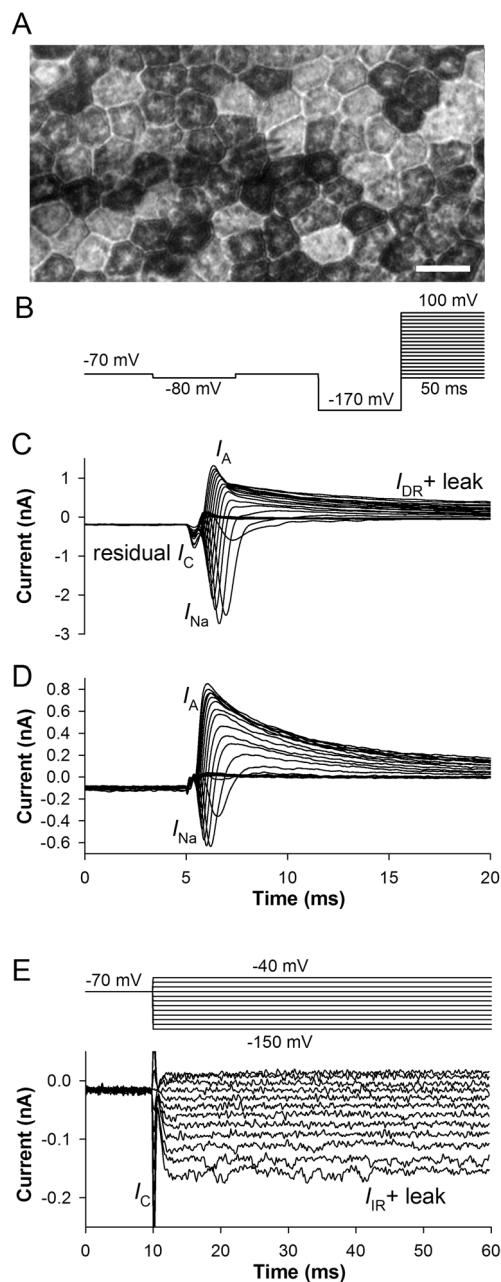
Ignatova *et al. BMC Biology*   (2023) 21:84

Page 3 of 19

Fig. 1 Ionic currents in hESC-RPE and their variability. **A** Bright-field microscopy image of hESC-RPE monolayer with the patch pipette attached to the cell. Scale bar is 10 µm. **B** Experimental protocol to record I_{Na}; a 50-ms pulse to −80 mV was given from a holding potential of −70 mV to measure leak current and membrane capacitance; a 50-ms pre-pulse to −170 mV was used to recover I_{Na} before stimulating with 50-ms testing pulses in 10 mV increments from −80 to 100 mV. **C**, **D** Examples of whole-cell currents recorded from two cells; I_C, residual capacitive current; I_{Na}, voltage-activated Na$^+$ current; I_A and I_{DR}, the transient and sustained outward voltage-activated K$^+$ currents, respectively. **E** An example of sustained hyperpolarization-activated inward current (I_{IR})

and slightly fluctuating I_C with I_{Na} as the activation kinetics of I_{Na} accelerated with depolarization. However, this complication was usually not present at voltages below 0 mV. I_{Na} activation threshold was in between −40 and −30 mV. The average current-voltage (*I–V*) relation for a group of cells without capacitive artifacts is shown in Fig. 2B. It can be seen that the current disappears by +80 mV, consistently with the +86 mV reversal potential for Na$^+$ created by the recording solutions (see "Methods").

In addition to I_{Na}, RPE can express voltage-activated Ca^{2+} channels that mediate an inward Ca^{2+} current with voltage dependencies similar to those of I_{Na} but slower kinetics [31, 32]. Because calcium currents in hESC-RPE appear to be very small and mostly non-inactivating, requiring replacement of Ca^{2+} ions by Ba^{2+} ions in the external solution for measurement [5], we did not investigate them specifically. However, we verified the consistency of I_{Na} characteristics without the contribution of K$^+$ and Ca^{2+} channels using Cs$^+$-based intracellular solution and 10 µM nifedipine extracellularly (Additional file 1. Fig. S1) [33].

Next, we determined voltage dependencies of several I_{Na} parameters. Availability of I_{Na} was investigated using a steady-state inactivation (SSI) protocol consisting of 50 ms conditioning pulses between −150 and −10 mV followed by a test pulse to 0 mV (Fig. 2C). As can be seen from the gradually decreasing I_{Na} during the test pulse, exposure to voltages in the range from *ca.* −120 mV to the I_{Na} activation threshold caused closed-state inactivation (Fig. 2C, D). The half-inactivation potential was −57.8 ± 4.4 mV (Fig. 2D). In particular, 27% of I_{Na} was on average available after a brief exposure to −50 mV and 11% after holding at −40 mV. Interestingly, I_{Na} time to peak decreased steadily with increasing voltage of the conditioning pulse, from 1.60 ± 0.30 ms after holding at −150 mV to 1.27 ± 0.21 ms after holding at −70 mV ($P = 10^{-11}$, paired *t*-test, Fig. 2C, D), indicating voltage-dependent facilitation of I_{Na}. This is probably caused by accumulation of Na$^+$ channels in the conformation states that promote both rapid opening and steady-state inactivation. The overlap between the voltage dependencies of activation (obtained from *I–V* relations, the half-activation potential of 23.1 ± 1.6 mV) and inactivation indicated that a small window current might exist around −35 mV (Fig. 2D).

Recovery from inactivation was evaluated at four membrane potentials (Fig. 2E–G). After a 50-ms pulse to 0 mV to activate and inactivate I_{Na}, the cell was exposed for variable durations to the test potential, from 0.5 to 21.0 ms in 0.5-ms increments. The resulting response series allowed measuring the time constant of recovery by fitting the time course of peak I_{Na} increase with a first-order exponential rise-to-maximum equation (Fig. 2E, F).
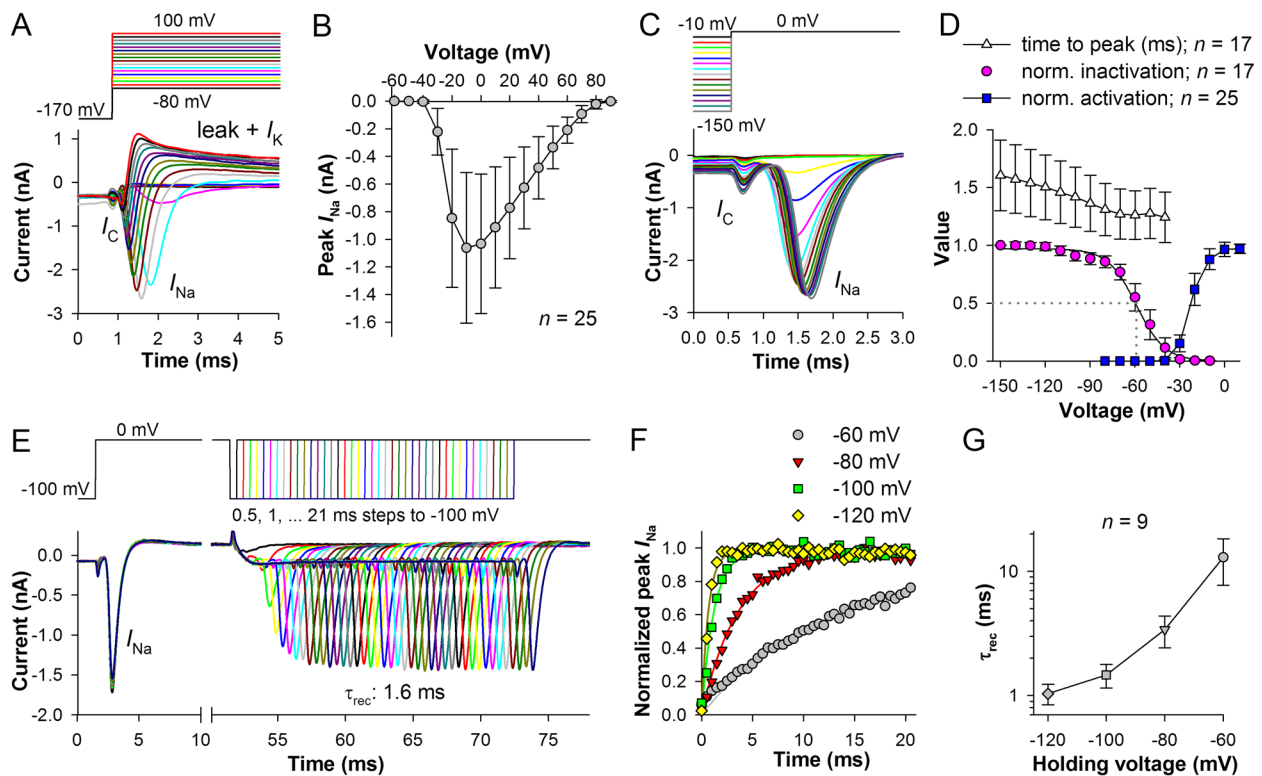
Fig. 2 Kinetics of voltage-activated Na$^+$ currents (I_{Na}). **A** Typical I_{Na}; I_C, residual capacitive current; I_K, the putative voltage-activated K$^+$ current. **B** Average current-voltage (I–V) relationship for I_{Na} ($n = 25$); here and elsewhere error bars are s.d. (Additional file 2: Table S1). **C** Steady-state inactivation (SSI) was studied by evoking I_{Na} at 0 mV after 50 ms conditioning pre-pulses from −150 to −10 mV. **D** Voltage dependencies of the average peak I_{Na} (circles) and its time to peak (triangles) from SSI experiments ($n = 17$), and voltage dependence of the normalized peak I_{Na} conductance ($n = 25$, squares). SSI data were divided by the amplitude of I_{Na} after the pre-pulse to −150 mV; in the figure, average values were fitted with a sigmoidal equation. Conductance at each membrane potential V was calculated using peak I_{Na} from I–V relations as in **B** and equation $g_{Na}(V) = I_{Na}/(V − E_{rev})$, where $E_{Na} = 85.8$ mV (Additional file 2: Table S1). **E** Recovery of I_{Na} from inactivation. I_{Na} was evoked and inactivated by 50-ms pre-pulses to 0 mV, after which hyperpolarizing pulses of increasing duration ranging from 0.5 to 21.0 ms were applied to recover I_{Na}; this was followed by a testing pulse to 0 mV. In these experiments, the holding potential between the trials and the recovery potential were the same. **F** By plotting peak I_{Na} during recovery from inactivation against the hyperpolarizing pulse duration and then fitting the data with a first-order exponential rise-to-maximum equation, recovery time constants (τ_{rec}) can be obtained; examples are from the same cell as in **E**. **G** Voltage dependence of average recovery time constants (Additional file 2: Table S1)

Time courses of recovery with exponential fits are shown for one cell in Fig. 2F. Figure 2G demonstrates the average voltage dependence of recovery time constants. I_{Na} recovered with the time constant of 1.05 ± 0.26 ms at −120 mV but only 16.9 ± 6.7 ms at −60 mV.

Spikes in the current-clamp experiments

The presence of I_{Na} in hESC-RPE raises an immediate question about the capability of RPE cells to generate transient depolarizations, such as action potentials or spikes. To further investigate their electrophysiological properties in general and voltage spiking in particular, we used several current-clamp protocols, all of which contained a hyperpolarizing current injection to recover I_{Na} prior to a test stimulus. The duration of such

hyperpolarizing pulses was set to 50 ms and amplitude varied depending on the membrane resistance in order to hyperpolarize membrane potential to below −100 mV to quickly recover most of I_{Na} (Fig. 2G).

Figure 3A shows ionic currents and Fig. 3B voltage responses to a series of depolarizing current pulses recorded in the same cell. Spikes appeared when membrane was depolarized to above −40 mV, with their times to peak decreasing with depolarization. Another important feature was that in the absence of spikes, the RPE membrane behaved like a passive electrical circuit, i.e., the time course of charging could be easily fitted with a first-order exponential function (see the stable membrane resistance in Fig. 3E).

To study the properties of spikes, it was necessary to separate them from the underlying voltage responses. We used a procedure described in Fig. 3C. The spike distorts

Ignatova *et al. BMC Biology*   (2023) 21:84

Page 5 of 19

the rising phase of the voltage response causing a deviation from the uniform exponential rise to maximum. By removing the spike-containing part of the trace and fitting the rest with a first-order exponential rise-to-maximum equation, an estimate of a response without the spike can be obtained (Fig. 3C, red trace). By subtracting it from the original trace, the spike waveform is acquired (Fig. 3C, green trace). Spikes from Fig. 3B are shown in Fig. 3D and their properties are described in Fig. 3E, F. Spike amplitude changed little with depolarization, unlike the amplitude of I_{Na} (Fig. 3E). In contrast, spike time to peak decreased strongly with depolarization, similarly to changes in the time to peak of I_{Na} (Fig. 3A), albeit in a much wider temporal range due to the relatively slow membrane charging in the current-clamp experiments. Kinetics of spikes, including the 25–75% rise and decay times, also accelerated, resulting in a gradual narrowing of spikes with depolarization (Fig. 3F). Because membrane was passive in the studied voltage range, these differences could be attributed to voltage dependence of I_{Na} kinetics.

Although evidence suggested that spikes are caused by I_{Na}, it was necessary to perform a definitive test. We used 10 µM TTX to block I_{Na} and evaluate changes in spikes (Fig. 4). TTX strongly suppressed I_{Na} (Fig. 4A). Simultaneously, spike amplitudes decreased dramatically and clearly in proportion to changes in the peak I_{Na} (Fig. 4B, C). This was observed in all three experiments ($P = 0.02$ for both I_{Na} and spike amplitude, paired t-test, Fig. 4D). These results unequivocally prove that spikes are mediated by I_{Na}.

Next, we investigated the voltage dependence of spikes. Figure 5A–C shows a representative experiment. The cell was stimulated with 100 ms hyperpolarizing conditioning current pulses of different amplitudes to obtain membrane potentials in the range from below −120 mV (to fully recover I_{Na}) to about resting potential. The hyperpolarizing pulses were followed by relaxation to resting potential, which triggered the spikes, depending on the preceding membrane potential. The spike amplitude and time to peak decreased with depolarization, whereas the half-width increased (Fig. 5C). The decrease
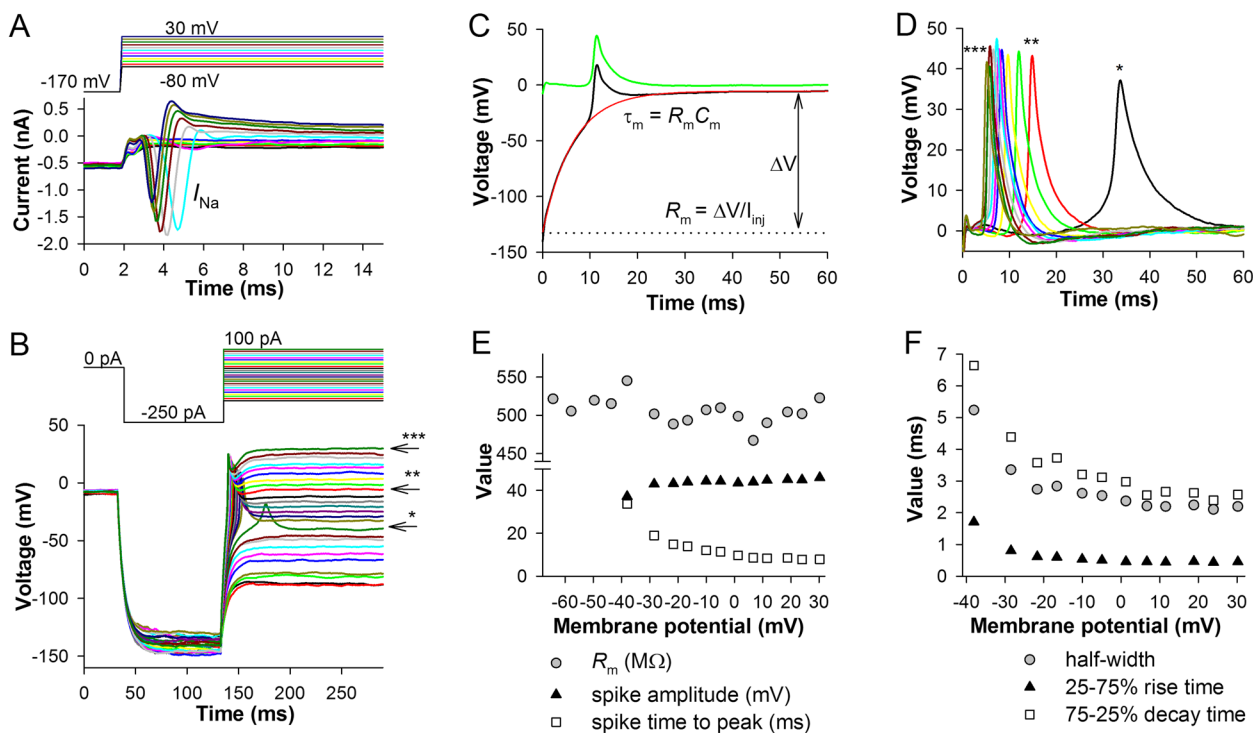

Fig. 3 Fast sodium spikes in current-clamp experiments. **A** Example of voltage clamp recordings. **B** Spikes in a current-clamp experiment were evoked by first hyperpolarizing the cell with 100-ms current injections to below −100 mV and then applying depolarizing pulses as indicated. **C** Separation of a spike (green trace) from the voltage response (black); the region containing a spike was excised and the remaining trace fitted with a first-order exponential rise-to-maximum equation (red); subtracting the traces elicited the spike. Membrane resistance (R_m) was determined from the amplitude of the voltage response (ΔV) to the injected current (I_{inj}); membrane time constant (τ_m) obtained by the fitting was used to calculate membrane capacitance (C_m) as indicated. **D** Examples of spikes; asterisks correspond to the marked traces in **B**. **E** Voltage dependencies of membrane resistance, spike amplitude, and spike time to peak in the same experiment; note that the membrane potential refers to the steady-state voltage reached *after* membrane charging is finished, which is in most cases higher than the potential at which the spike is initiated. **F** Voltage dependencies of spike parameters: half-widths, 25–75% rise and 75–25% decay times
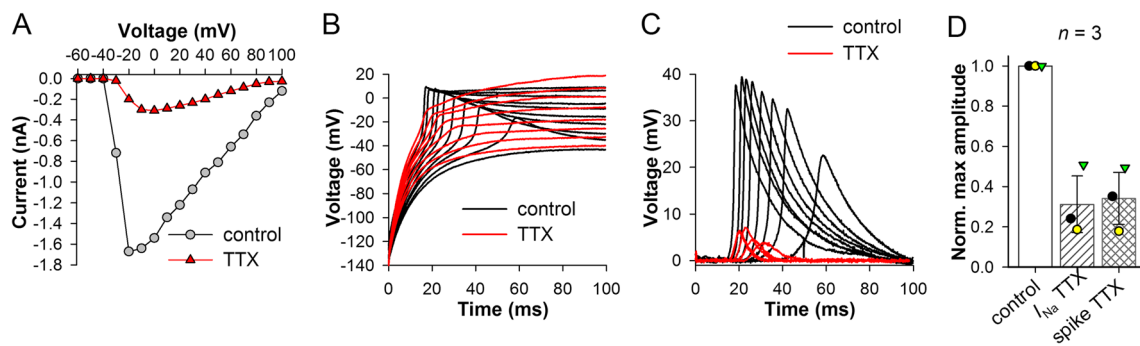
Ignatova *et al. BMC Biology*   (2023) 21:84

Page 6 of 19

Fig. 4 Effect of TTX on I_{Na} and spikes. **A** I–V relations from an experiment involving inhibition of I_{Na} with 10 μM TTX. **B** Traces of current-clamp recordings in control conditions with spikes visible and after application of TTX from the same cell as in **A**; data were obtained as described in Fig. 3B; stimuli not shown. **C** Isolated spikes from **B**. **D** Summary of TTX experiments. Amplitudes of the largest I_{Na} and spikes were measured in three cells before and after application of TTX; values in the presence of TTX were divided by control ones and averaged (Additional file 2: Table S1)
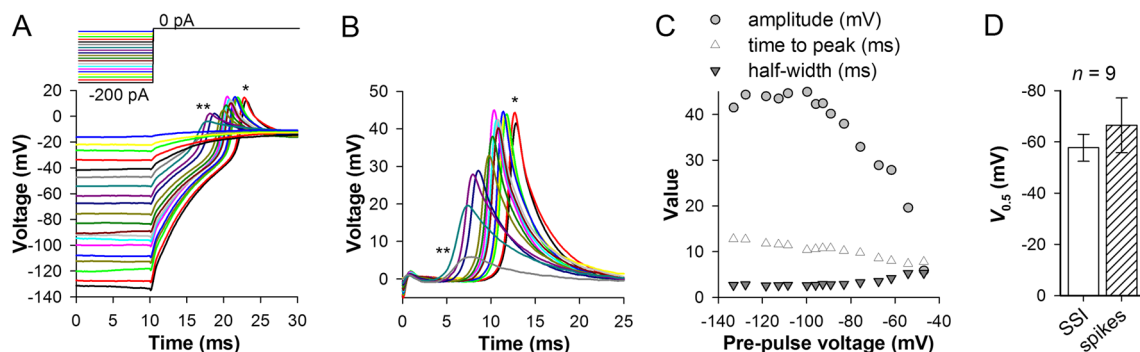

Fig. 5 Voltage dependence of spikes. **A** Voltage responses of an RPE cell at resting potential after a series of 100-ms conditioning hyperpolarizing pre-pulses. **B** Isolated spikes from **A**, with asterisks indicating the correspondence between spikes in **A** and **B**. **C** Dependence of spike amplitude, time to peak and half-width on the pre-pulse voltage; data from **A** and **B**. **D** Comparison of the average half-inactivation potentials from SSI recordings and the average half-maximal amplitude potentials for spikes (both denoted with $V_{0.5}$) in the same cells; the voltage dependencies were fitted with a sigmoidal equation (Additional file 2: Table S1).

in amplitude was due to closed-state inactivation of I_{Na} as the consistent average half-inactivation potential for I_{Na} and the half-maximal spike amplitude potential indicate (Fig. 5D). The decrease in the time to peak was due to a comparatively fast membrane charging toward the I_{Na} activation threshold from more depolarized conditioning potentials.

Because voltage-gated K$^+$ conductances can condition spikes caused by I_{Na}, and also because activation of delayed rectifier K$^+$ conductances by a depolarizing current injection can cause spike-like voltage transients [34], we correlated spike sizes and half-widths with the amplitudes of I_{DR} and I_A. The currents were measured after a 50-ms pre-pulse to −170 mV at the nominal voltage pulse to +100 mV (see Fig. 1B). I_A was measured as the difference between the peak outward current and the sustained current at the end of 50-ms pulses. I_{DR} was determined at the end of 50 ms pulses, with leak subtracted. We found a weak positive correlation ($r = 0.2$, P

= 0.019, $n = 140$) between I_A and spike amplitudes but no correlation between I_{DR} and spike amplitudes. No correlations could be found between I_A and I_{DR} amplitudes, on the one hand, and spike half-width, on the other hand.

In contrast, the maximal spike amplitude correlated strongly with the peak I_{Na}, with $r = -0.66$ (Fig. 6A, $n = 95$). Figure 6B clearly shows that the distribution of peak I_{Na} was not Gaussian, with a median of −1140(−765:1635) pA ($n = 105$).

However, membrane charging by I_{Na} during the onset of the spike depends not only on I_{Na} amplitude but also on its density. Figure 6C shows that capacitance, a proxy for cell membrane area, varied substantially in our experiments. The distribution was also not Gaussian, with a median of 17.1(11.6:21.9) pF ($n = 99$). The correlation between the maximal spike amplitude and I_{Na} density obtained by dividing peak I_{Na} by C_m (Fig. 6D) was −0.72, stronger than that in Fig. 6A.
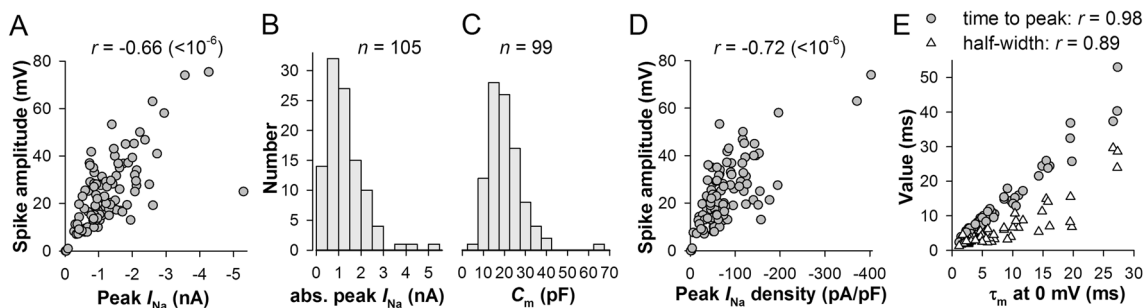
Fig. 6 Spikes, I_{Na} and membrane time constant. **A** Correlation between the maximal spike and I_{Na} amplitudes; I_{Na} was measured from a recording immediately preceding the current-clamp. **B**, **C** Distribution of maximal I_{Na} amplitudes (**B**) and C_m values (**C**); the distributions are not Gaussian (P < 0.001, Shapiro-Wilk normality test). **D** Correlation between the maximal spike amplitudes and I_{Na} densities; I_{Na} density was obtained by dividing peak I_{Na} with the corresponding C_m value. **E** Plots of spike time to peaks and half-widths against membrane time constants; the spikes were obtained from voltage responses reaching the level of ca. 0 mV (-0.9 ± 2.7 mV, $n = 60$) from voltages below -100 mV (-131 ± 21 mV, $n = 60$); the correlations were characterized by P values of $< 10^{-6}$

Speed of membrane charging varied between cells and often in the same cell during prolonged recordings (see next section). To test how variability in membrane time constant could affect the spike, we correlated spike properties to the corresponding time constants. Although membrane time constant (τ_m) did not depend on membrane potential, I_{Na} did, and so in the following analysis we used spikes obtained from voltage response traces with sustained potentials at around 0 mV and evoked from voltages below -100 mV to minimize closed-state inactivation of I_{Na}. There was no correlation between spike amplitude and τ_m ($r = 10^{-2}$), i.e., the speed of membrane charging had no effect on the spike size. However, a nearly unity (0.98) correlation was discovered between τ_m and spike's time to peak (Fig. 6E), and a less strong correlation ($r = 0.89$) was observed between τ_m and spike's half-width (Fig. 6E). The latter correlation was caused by strong dependencies on τ_m of spike's 25–75% rise and decay times, with the corresponding correlation coefficients of 0.74 and 0.88 (for both, $P < 10^{-6}$; $n = 60$).

Although we did not register spontaneous spikes when membrane potential was not hyperpolarized by current injections, there is evidence that they can be evoked if membrane potential transiently decreases to recover a sufficient fraction of I_{Na}. Figure 7A demonstrates three traces recorded in a current-clamp experiment. The red trace contains a spike (arrow) triggered by a sharp spontaneous depolarization after a brief hyperpolarization (two asterisks). The same trace also contains episodes of rapid depolarization (asterisks), which, however, failed to trigger spikes. Immediately after the spontaneous spike, the hyperpolarizing current pulse was switched off and the cell depolarized to about 0 mV (Fig. 7B). Because available Na^+ channels were inactivated during the spike, no new spike could be elicited, in contrast to the other two traces (black and green), where spikes did appear.

In another experiment, I_{Na} was large, had a low activation threshold, and its substantial fraction ($\sim$20%) was available after a 50 ms exposure to -40 mV (Fig. 7C, white triangles). Figure 7D shows three voltage traces from the associated current-clamp recording. A large spontaneous spike can be seen on the black trace (arrow). Its activation threshold was about -60 mV and, by comparison with two other traces characterized by the similar membrane potential, it appears that the spike was evoked because a substantial fraction of I_{Na} recovered during the preceding hyperpolarization between 220 and 310 ms.

Figure 7E illustrates the stochasticity of spike amplitudes and kinetics when they were triggered around the I_{Na} threshold potential in another RPE cell. Seven traces are shown. Clear spikes can be seen in four traces during two depolarizing segments. No spike appeared in the black trace, although during the second depolarizing segment a slow transient was evoked. This trace was characterized by the most positive membrane potentials before the depolarizing pulses, so that 97% of the maximal I_{Na} was available before the first and 84% before the second depolarizing segment (values from the associated SSI recording). Similarly, no spike was evoked during the red trace characterized by even more hyperpolarized potentials. Green and cyan traces almost coincided with each other and with the red trace in their pre-depolarization membrane potential but only the green trace had clear spikes. Likewise, gray and blue traces were quite similar in their membrane potentials, but spikes appeared only on the blue trace. Two spikes can be seen in the pink trace but their timing relative to other spikes was different during the two depolarizing segments.

Although we found no clear spikes at resting membrane potential (V_{rest}) in our recordings, any residual I_{Na} persisting at V_{rest} or recovered by a preceding hyperpolarizing fluctuation of membrane potential can plausibly
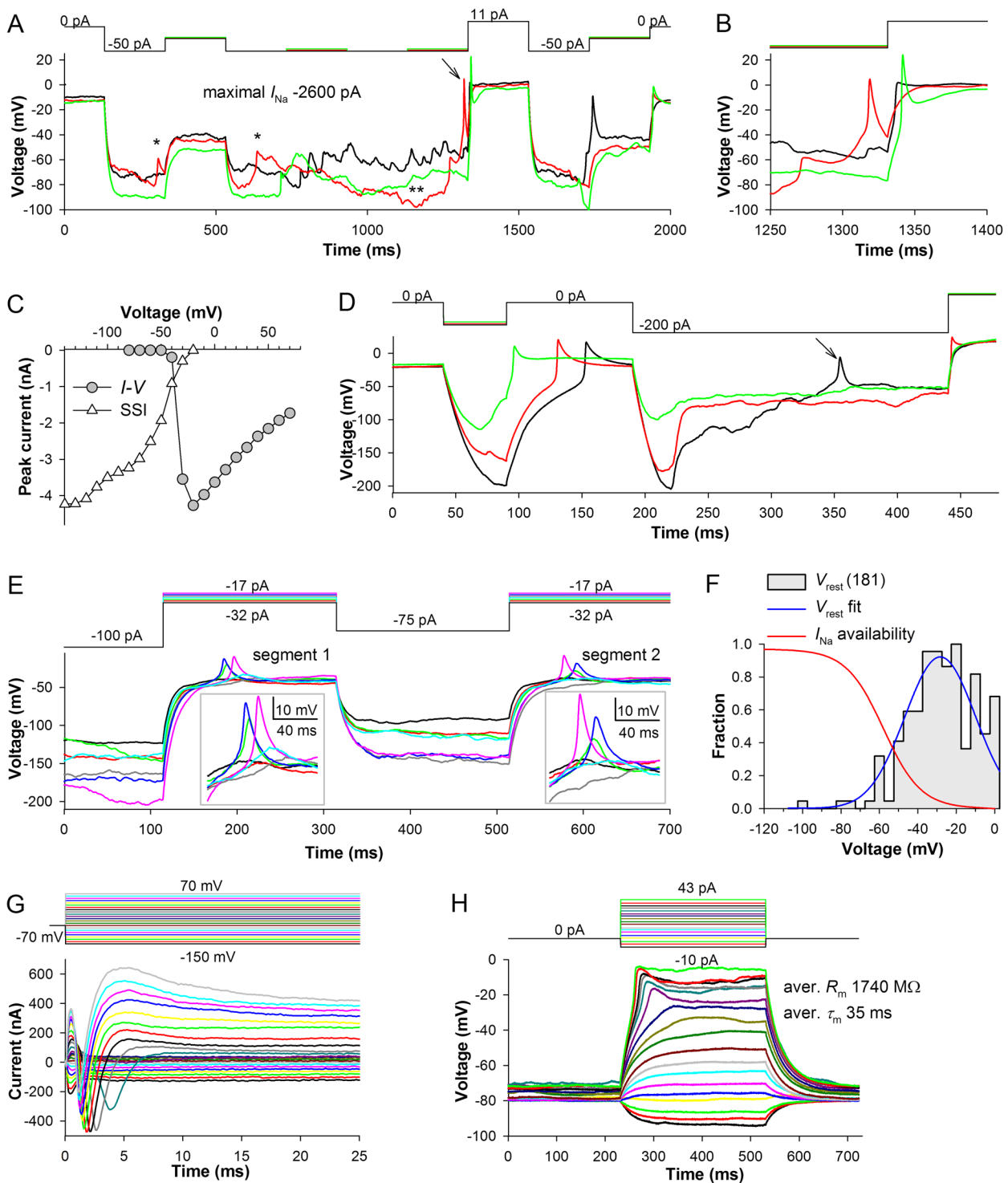
Fig. 7 Stochasticity of spike onset. **A** Spikes can occur apparently spontaneously when the cell is hyperpolarized by current injection; asterisks denote two particularly sharp depolarizing transients and the double asterisk the region of spontaneous hyperpolarization preceding the actual spike (arrow). **B** Magnified spike-containing segment from (**A**). **C** *I–V* and SSI relations for another cell characterized by a large I_{Na} with a comparatively negative I_{Na} activation threshold. **D** Parts of three voltage traces from a current-clamp recording, with a spike at 360 ms on the black trace. **E** Variability in spike properties in the I_{Na} activation threshold region. **F** Distribution of minimal resting potentials, its Gaussian fit, and the I_{Na} availability curve obtained by fitting the SSI data from Fig. 2D; the V_{rest} histogram data were divided by the maximum value. **G**, **H** Ionic currents (**G**) evoked from a holding potential of −70 mV in an RPE cell with a very negative V_{rest} and the associated current-clamp recording (**H**)

Ignatova *et al. BMC Biology* (2023) 21:84

Page 9 of 19

amplify the next rapid depolarizing fluctuation. The resulting transient might resemble the smallest dark gray spikelet in Fig. 5B or the fast depolarizing spikelets on the red and black traces in Fig. 7A. To estimate the available fraction of I_{Na} at rest in the experimental group, we plotted the histogram (Fig. 7F) of the most negative V_{rest} values obtained in each cell in the absence of current injection (e.g., from the green trace in Fig. 7A at 0 ms or the black trace in Fig. 9 at 0 ms). The average V_{rest} was -29 ± 18 mV (181 cells), which would become -42 mV after the liquid junction potential error correction. The histogram was fitted with a Gaussian equation (blue trace) and superimposed on the SSI fitting curve from Fig. 2D (red trace). In the minority of cells characterized by V_{rest} below -50 mV, more than 40% of I_{Na} could be available. However, in the majority of cells, I_{Na} at V_{rest} was inactivated almost completely.

An example of a cell with a very low V_{rest} is shown in Fig. 7G, H. The currents were recorded from a holding potential of -70 mV. Figure 7G shows comparatively large I_{Na}, I_A, I_{DR}, I_{IR}, and a small leak current in the vicinity of V_{rest}. In the current-clamp measurements, V_{rest} occasionally reached -80 mV, indicating the availability of a large fraction of I_{Na}. Consequently, upon stimulation with depolarizing current injections, spikes were elicited after crossing the I_{Na} activation threshold at about -40 mV. The low V_{rest} was associated with very high average R_m of 1730 MΩ and membrane time constant of 35 ms, which could explain the stability of membrane potential and absence of fluctuations.

Dynamic changes in membrane resistance

Figure 3 shows current-clamp recordings characterized by relatively stable R_m (Fig. 3E) and V_{rest} values (Fig. 3B). However, such stable recordings were exceptions rather than a rule because R_m and V_{rest} tended to change continuously. Figure 8A, B demonstrates parts of two recordings from the same cell, both displaying large spikes (Fig. 8C, D). During the recording in Fig. 8A, the cell had relatively small τ_m (Fig. 8E) and R_m (Fig. 8F), on average 222 MΩ. To charge its membrane potential to below -100 mV, a comparatively large hyperpolarizing current of -500 pA was needed (top).

In contrast, the recording in Fig. 8B was characterized by large τ_m (Fig. 8E) and R_m (Fig. 8F), and a small -100 pA current hyperpolarized membrane potential to below -100 mV. The relatively low-resistance green trace in Fig. 8B illustrates sudden changes in R_m during the recordings (each trace is a part of a 1-s recording). Importantly, while the average R_m and membrane time constant increased by threefold, the average C_m did not change (Fig. 8E), supporting the validity of our estimation procedure (Fig. 3C). The differences in the properties

of spikes (Fig. 8C, D) were consistent with the findings shown in Fig. 6E: changes in membrane time constant had a small effect on the spike amplitude but strongly altered their times to peak, half-widths, and kinetics.

Top plot of Fig. 8G shows an example of periodic changes in R_m over the course of a prolonged experiment consisting of many current-clamp recordings. R_m varied from 60 to 3900 MΩ, which corresponded to changes in membrane conductance from 17 to 0.26 nS. Comparison of time courses of changes in R_m and V_{rest} (Fig. 8G, bottom) indicated that V_{rest} depolarized when R_m decreased and vice versa. This implies that the fluctuating membrane leak was depolarizing, i.e., mediated by an inward cationic or outward anionic current. Figure 8H shows V_{rest} values plotted against the respective R_m values for the whole experiment in Fig. 8G, and Fig. 8I–K demonstrates similar plots for three more experiments. All results were consistent: V_{rest} was a function of membrane leak.

Although changes in R_m and V_{rest} usually occurred gradually, they were often facilitated by strong and sudden membrane depolarization or hyperpolarization. Figure 9 shows two examples of rapid hyperpolarization-induced decreases in R_m. Over the course of the black trace, the cell was first characterized by a comparatively negative V_{rest} and high R_m, >1100 MΩ. Even before the membrane potential had fully settled during a -250 pA current pulse, a sudden decrease in R_m, to ~350 MΩ, happened at 62 ms. Eventually, after the decrease in R_m at ~370 ms, the cell acquired a resistance of 140 MΩ. Accordingly, V_{rest} increased from -32 mV at the trace onset to $+2$ mV at 650 ms. The second negative transient, with the corresponding R_m estimates, can be seen on the red trace at 670 ms.

Multiple waves of excitation

In 19 out of 707 studied cells, in addition to the conventional I_{Na}, we found anomalous secondary depolarizing currents (Fig. 10A) characterized by relatively large times to peak, with slow onsets and inactivation kinetics. The currents were clearly voltage-dependent.

To investigate the properties of these delayed inward currents, we separated them from the outward current using a procedure similar to that we used to isolate spikes (Fig. 3C). Comparison of the $I–V$ relations for I_{Na} and the delayed inward current showed that the extrapolated reversal potential of the new current should be extremely positive (*ca.* +200 mV, Fig. 10B). In the current-clamp experiments, the delayed inward current caused secondary spikes (Fig. 10C). Similarly to the closed-state inactivation of I_{Na} (Fig. 2D), the delayed inward current is inactivated by pre-exposing the cell to the same range of membrane potentials.
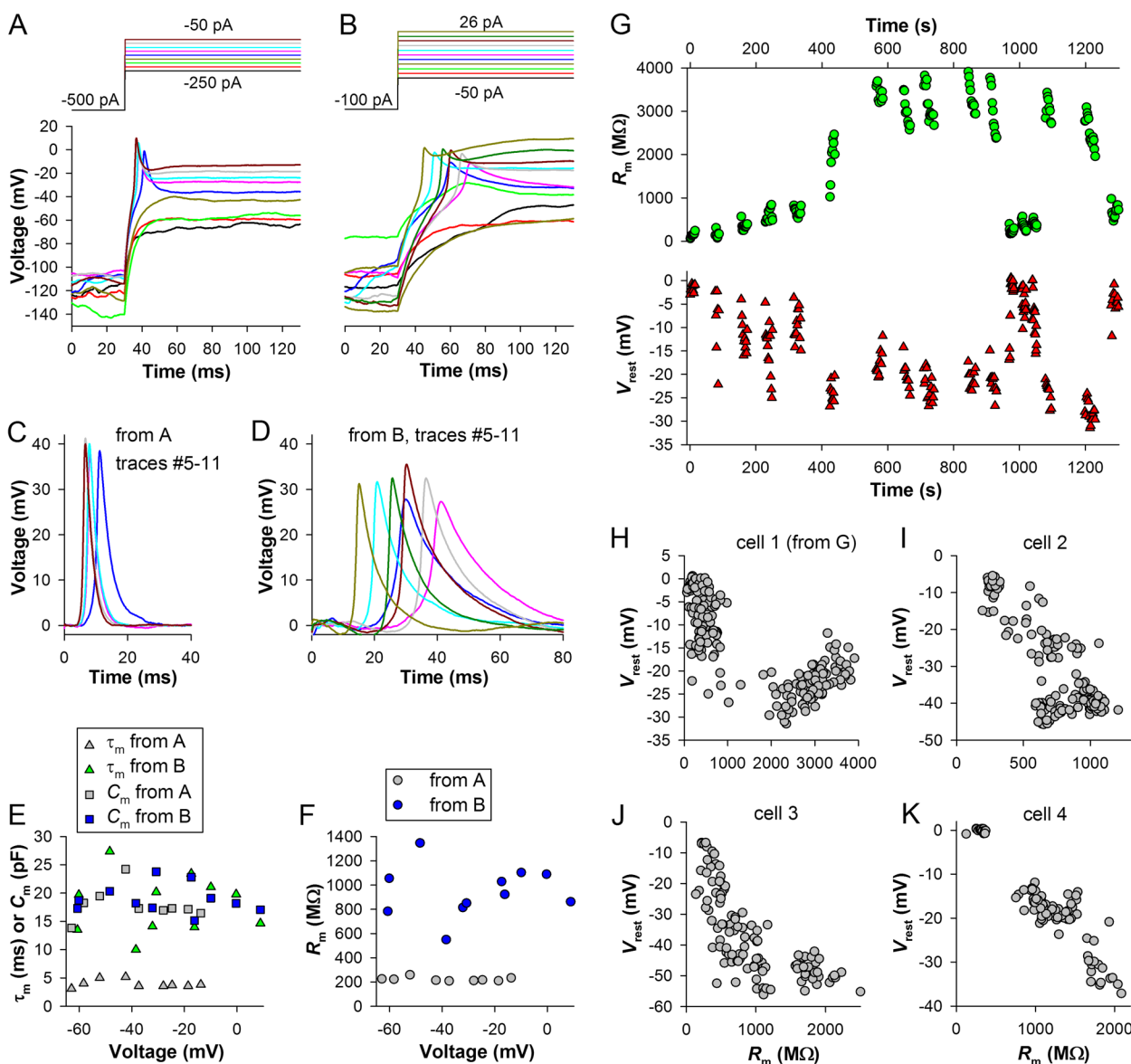
Fig. 8 Spontaneous changes in leak conductance and its effects. **A**, **B** A recording with a low R_m (**A**) was followed by a recording with a relatively high R_m (**B**); **C**, **D** Spikes from the low- (**C**) and high-resistance (**D**) recordings; color coding is the same as in **A** and **B**, respectively. **E** Dependencies of membrane time constants and capacitances on the response voltage immediately after the spike. **F** Dependencies of membrane resistances on the response voltage immediately after the spike; **A–F**, data from the same cell. **G** Time courses of changes in R_m (top) and resting potential V_{rest} (bottom) during one experiment. **H–K** Correlations between R_m and V_{rest} during similarly prolonged recordings in 4 cells

Surprisingly, detailed examination of several recordings characterized by the presence of the second inward current revealed additional delayed inward currents (Fig. 10D–G). In Fig. 10D, the third inward current (inward 3) was small and even more delayed and slower than the second one (inward 2), eliciting small and slow depolarizations (Fig. 10F). In this cell, the second inward current I–V relation (Fig. 10E) had apparently a similarly positive reversal potential as the delayed inward current

in Fig. 10A, B, whereas the I–V relation for the third current could not be reliably estimated beyond +70 mV. It should be noted that the cells with delayed inward currents tended to have unusually high C_m values (see the prolonged membrane charging in Figs. 10A, D, G and 11A–C, G–I), which could not be compensated properly, hence the nominal voltage in I–V relations was probably a large overestimation. Membrane capacitance estimated in the voltage clamp recordings from the charge during
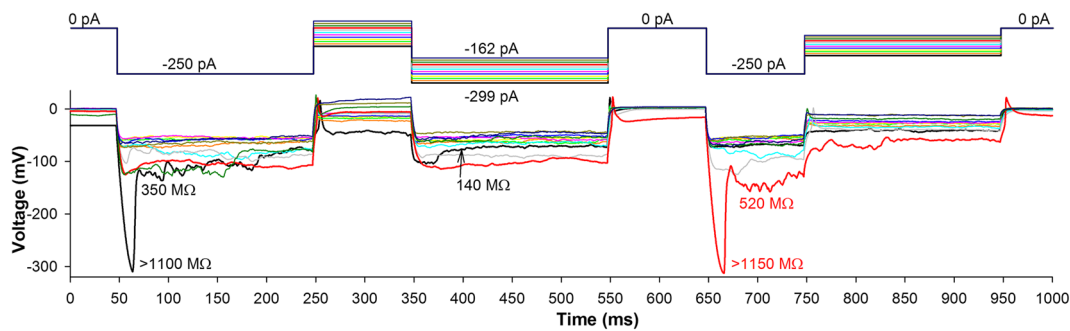
Fig. 9 Sudden changes in leak conductance. While leak conductance can change gradually, in some cases its decrease occurs suddenly in the beginning of a hyperpolarizing pulse, manifesting in a sharp hyperpolarizing transient. R_m values in black font refer to the black trace and in red to the red trace

the capacitive transient was on average 54(29:69) pF ($n = 19$) in the cells with the secondary delayed inward current but only 26(21:34) pF ($n = 685$) in the typical cells ($P < 10^{-3}$, Mann–Whitney U-test).

Figure 10G shows voltage clamp recording from a different cell with four depolarizing inward currents. Three inward currents were present at all potentials, except the threshold one, where the conventional I_{Na} and the first delayed inward current partly merged. The inward current 4 in Fig. 10G was small and slow, resembling the Fig. 10D current, and appeared at more positive potentials than the inward currents 1–3.

The presence of multiple depolarizing currents rules out a possibility of their origin in the same cell. This phenomenon can only be explained by the spread of excitation in both voltage- and current-clamp experiments to the neighboring cells via open gap junction channels. Consistently with this hypothesis, we found that the delayed inward current can be regulated dynamically, as shown in Fig. 10H. In six cells, it disappeared completely within minutes after the start of voltage clamp recordings.

Furthermore, gap junction conductance can be increased by lowering internal calcium concentration and vice versa [35]. Because L-type Ca^{2+} channels are expressed in hESC-RPE and are partly open at their typically depolarized resting potentials [5], we attempted to alter the internal calcium homeostasis by blocking these channels with nifedipine, which at 10 μM abolishes most of L-type Ca^{2+} channel current [5]. We recorded from five cells exhibiting delayed inward currents. Surprisingly, delayed inward currents increased noticeably immediately after application of 10 μM nifedipine. Figure 11A–C shows the effect of nifedipine in one cell. The effect was fully reversible (Fig. 11C, D). Bar plot in Fig. 11E summarizes the results of the experiments: on average, the maximal delayed inward current increased by more than 2-fold.

If nifedipine facilitates opening of gap junctions, then this can manifest in changes of C_m. However, because the gap junction conductance status in control cells is not known, we compared C_m in the presence of 10 μM nifedipine to that after wash-out of nifedipine and application of connexin 43 (Cx43) channel inhibitor 18α-glycyrrhetinic acid (18α-GA). Cx43 is the most abundant gap junction protein in human RPE [11, 17]. We used 10 μM concentration of 18α-GA, which, while only partly blocking gap junctions, does not cause irreversible effects [36]. Membrane capacitance measured in the voltage clamp decreased slightly but statistically significantly, from 29.0 ± 5.5 pF in the presence of nifedipine to 27.3 ± 5.2 pF after application of 18α-GA ($n = 6$; $P = 0.002$, paired t-test, Fig. 11F). It should be noted that these measurements were conducted on cells that displayed no delayed inward currents.

In one cell with a delayed inward current, application of 10 μM 18α-GA caused a decrease in C_m and a simultaneous decrease in the delayed current but did not affect the amplitude of the primary I_{Na} (Fig. 11G, H). When 18α-GA was washed out and replaced with TTX, C_m returned to the control value while the amplitudes of both inward currents decreased (Fig. 11 I). The results of this experiment summarized in Fig. 11J are consistent with the hypothesis that the delayed inward currents originate in the neighboring cells and are mediated by I_{Na}, with signals spreading via gap junction channels.

Discussion
In this work, we (1) described Na^{+}-based voltage spikes in hESC-RPE cells, (2) documented rapid spontaneous changes in membrane conductance and resting potential, and (3) discovered that electrical excitation can spread to the neighboring cells in a syncytium comprised of the conventionally non-excitable cells.
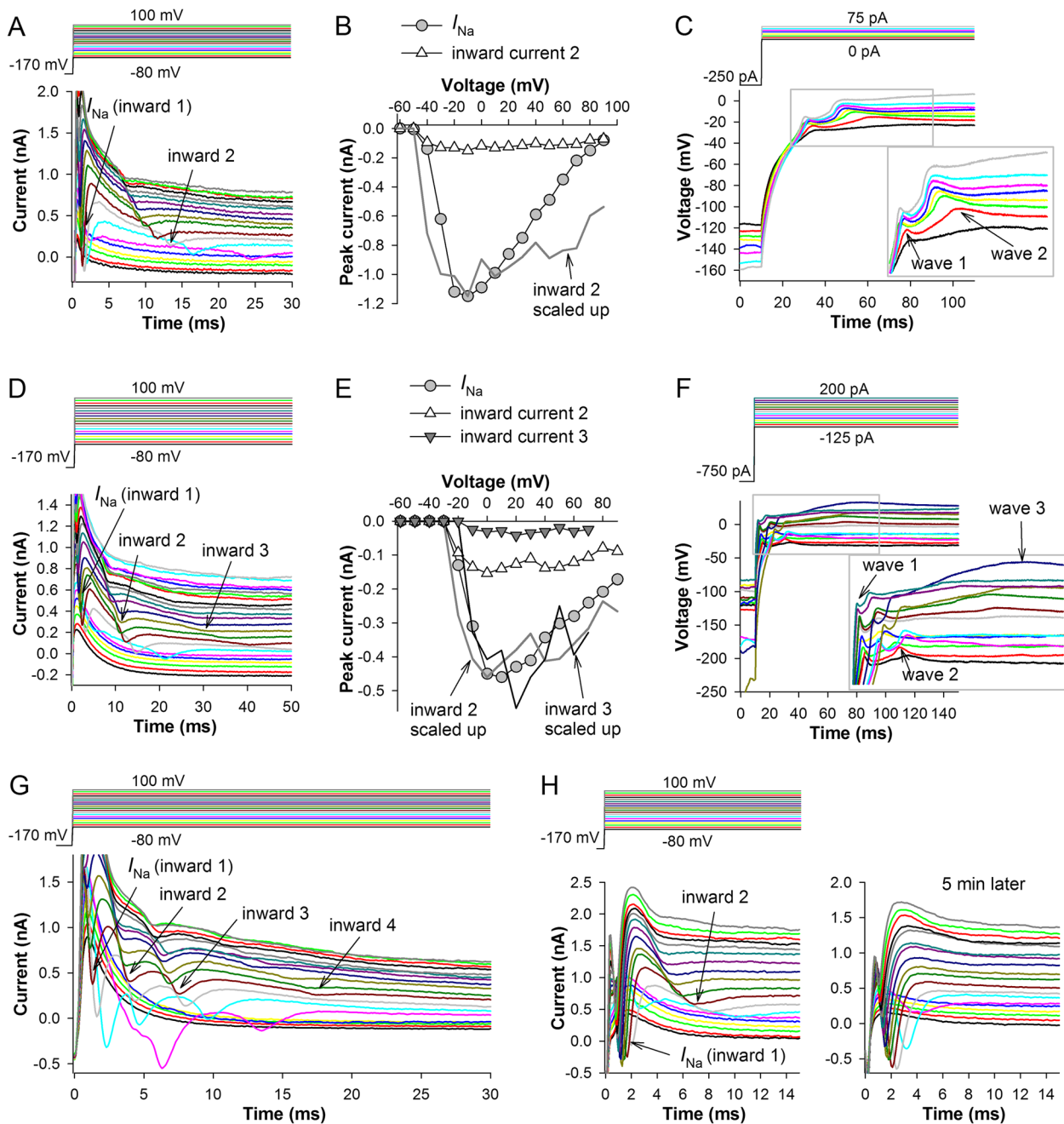
Fig. 10 Multiple inward currents. **A** Voltage clamp recording with two depolarizing currents, a conventional I_{Na} (inward 1) and a relatively small and slow delayed inward current (inward 2). **B** The I–V relations for the two currents and the scaled up inward 2 current; inward 2 current was isolated by (1) removing the delayed current-containing part of the trace, (2) fitting the remaining trace between 5 and 30 ms with a polynomial equation, and (3) subtracting the fitting curve from the original trace. **C** A current-clamp recording from the same cell with two types of voltage spikes that correspond to the currents in **A**. **D–F** A recording from another cell, **D** with three waves of inward currents, **E** the corresponding I–V relations, and **F** the current-clamp recording. **G** Example of four inward currents from a different cell. **H** An example of recordings where the delayed inward current (inward 2, left) disappeared spontaneously after 5 min of recordings (right)

Spikes

Expression at significant levels of the classical voltage-activated Na⁺ conductances characterized by ultra-fast activation and inactivation is usually associated with generation of voltage spiking events, ranging in amplitude from small depolarizing waves to full-blown action potentials. Fast depolarizing voltage responses resembling action potentials have been previously described
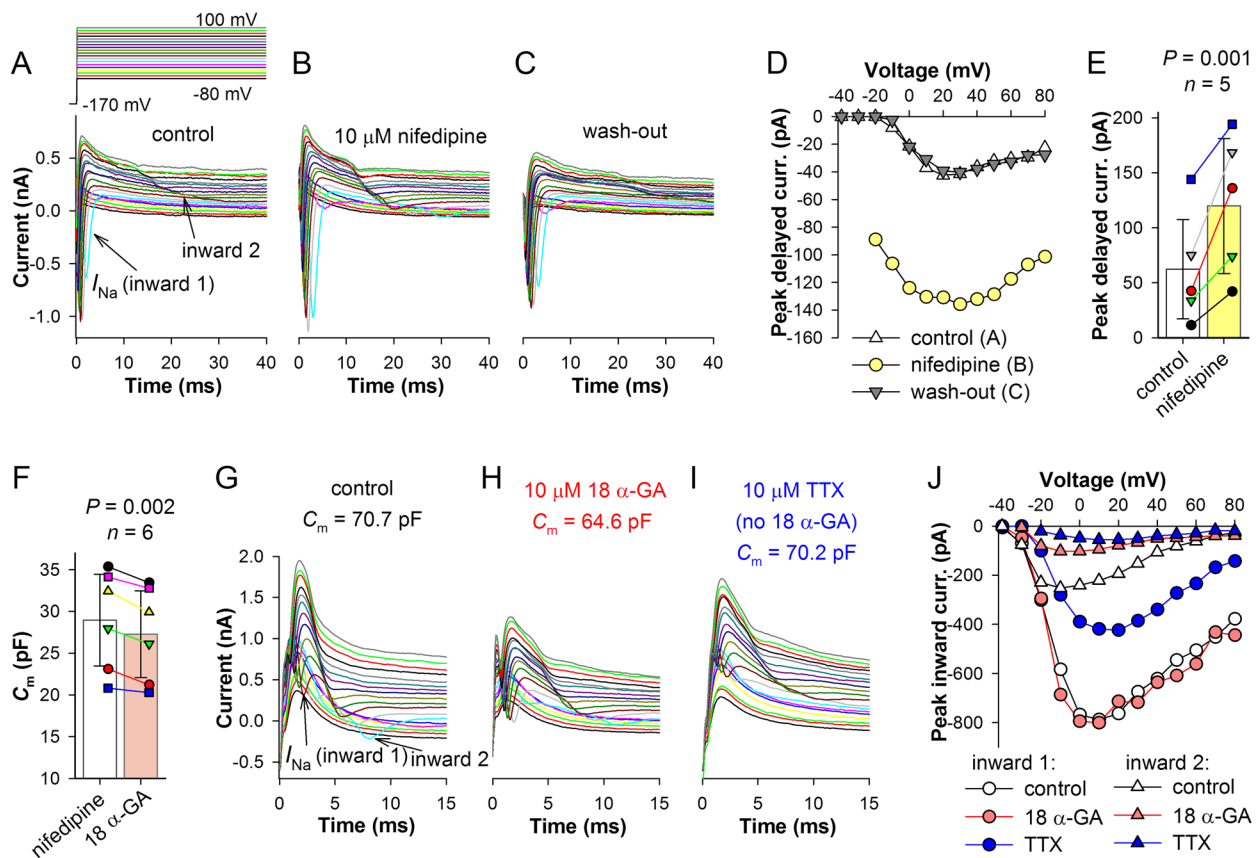
Fig. 11 Effects of nifedipine and 18α-GA on the delayed inward current. **A**–**C** Voltage clamp recordings in control conditions (**A**), after application of 10 μM nifedipine (**B**), and after wash-out (**C**). **D** *I*–*V* relations for the delayed inward currents from **A** to **C** (inward 2). **E** Bar plot summarizes changes in the peak delayed inward current in 5 cells in the presence of 10 μM nifedipine; paired *t*-test was used for the statistical comparison. **F** Cells were first exposed to 10 μM nifedipine and then, after wash-out of nifedipine, to 10 μM 18α-GA; bar plot shows changes in C_m ($n = 6$; $P = 0.002$, paired *t*-test). **G**–**J** Voltage clamp recordings in control conditions (**G**), after application of 10 μM 18α-GA (**H**), and, after wash-out, 10 μM TTX (**I**); **J** *I*–*V* relations for this experiment. In panels **F**–**J**, recordings were performed with Cs^+ in the pipette solution

in the conventionally non-excitable cells such as astrocytes [20–22], rabbit pigmented ciliary epithelial cells [23], newt RPE [19], and neonatal rat RPE [16]. However, Botchkin and Matthews attributed the development of I_{Na} and the spiking to neuronal trans-differentiation of the cultured and actively proliferating RPE [16].

Previous studies documented expression of multiple types of voltage-activated Na^+ and Ca^{2+} channels both in the cultured hESC-RPE and freshly dissected mouse RPE [4, 5]. I_{Na} can be large, raising a question about possible electrogenic function of Na^+ channels in RPE. In comparison to the previous study [4], the patch-clamp experiments in this work were performed with series resistance compensated and under conditions as close as possible to those the cells were maintained in, i.e. at the temperature of ~34°C, in the physiological medium and using "all-ions" intracellular solution, so that V_{rest} was not compromised by added K^+ channel blockers. We found that when I_{Na} was recovered from inactivation, depolarizing

current pulses indeed evoked spikes, the amplitudes of which were mainly determined by the maximal amplitude of I_{Na} (Fig. 6A, D). Application of TTX strongly inhibited both I_{Na} and spikes (Fig. 4).

We did not detect any spikes triggered spontaneously without prior manipulations with membrane potential. Our results indicate that spontaneous spike generation is precluded by low absolute availability of I_{Na} at normal V_{rest} values and high I_{Na} activation threshold when V_{rest} was permissive. The availability of I_{Na} is a function of the maximal I_{Na} and the momentary inactivation state. The spikes could not be evoked at the group-average V_{rest} of -29 ± 18 mV because of near complete I_{Na} inactivation. However, in nine cells (Fig. 7F), V_{rest} transiently hyperpolarized to the levels of <-60 mV, at which a major fraction of I_{Na} could recover from inactivation (Fig. 2D–G and 7F–H). Then, if the maximal I_{Na} was high enough to yield a sufficiently large residual I_{Na} at the V_{rest}, a depolarizing fluctuation of membrane potential could plausibly

trigger a spike as we observed in the current-clamp experiments (Fig. 7). Although we routinely detected spontaneous fluctuations of V_{rest}, a particularly large and rapid one would be required to reach the I_{Na} activation threshold potential at around −40 mV without a fatal loss of I_{Na} due to closed-state inactivation. Thus, a combination of several low-probability events is necessary to evoke a distinct spontaneous spike: a large I_{Na} expression level, several tens of ms long hyperpolarization to about −70 mV, and a rapid depolarization by about 30 mV (Fig. 7H).

Observations of V_{rest} fluctuations associated with changes in the putative depolarizing leak conductance (Fig. 8) suggest that addition of even a small repolarizing K^+ conductance might be sufficient to permanently lower V_{rest}. If hESC-RPE cells expressed sufficient quantities of conventional voltage-activated K^+ channels [18] supporting sustained current with a low voltage activation threshold, group-average V_{rest} would be more hyperpolarized. This would not only increase availability of I_{Na} but also make the membrane faster, enabling rapid voltage transients. For instance, the cell in Fig. 7G, H is characterized by a very negative V_{rest} because the depolarizing leak conductance is presumably very small whereas R_m is high. Any transient depolarization can be filtered out by the very slow membrane, preventing rapid reaching of the I_{Na} activation threshold.

Interestingly, V_{rest} of the freshly isolated adult human and monkey RPE was on average −50 mV [12], being in similar range in mouse RPE monolayers [17], that is ~20 mV lower than in our hESC-RPE (differences in liquid junction potentials accounted for). Contributing to V_{rest}, these cells also had prominent inward and delayed rectifier K^+ channels [12] and expressed I_{Na}, albeit only in subconfluent cultures [13] similarly to newt RPE [19]. Although the latter observation suggested that I_{Na} could be a feature of immature RPE [13], the recent findings demonstrate that Na^+ channels in mature hESC- and mouse RPE monolayers are largely localized in the vicinity of the cell-cell junctions [4]. Dissociation of RPE destroys the intercellular contacts and drastically decreases whole-cell I_{Na} [4]. Therefore, the observed differences between the freshly isolated and the cultured RPE cells require caution in interpretation of results [4, 13, 16].

Although full-fledged spikes are one of the most spectacular excitation events in hESC-RPE, amplification of small transient depolarizations by the residual I_{Na} might be its main electrogenic function. Such depolarizations interspersed with hyperpolarizations are prevalent in our data (Figs. 7A and 9). As discussed previously, depolarizing I_{Na} could contribute by promoting the opening of slower L-type Ca^{2+} channels [37, 38]. Of Ca^{2+}-dependent

processes in the RPE, POS phagocytosis is a highly dynamic event requiring rapid actin remodeling for the phagocytic cup formation and phagosome ingestion (reviewed by [39]). As POS phagocytosis has been shown to depend on both L-type Ca^{2+} and Na^+ channels [4, 5, 40, 41], depolarizing I_{Na} could facilitate L-type Ca^{2+} channel opening in the RPE participating in the complex interaction of molecular players involved in the Ca^{2+} regulation of phagocytosis [2].

Light response decreases the sub-retinal K^+ concentration causing hyperpolarization [9] that together with large spontaneous fluctuations in the membrane resistance could trigger activation of I_{Na} in vivo and make RPE excitable, with excitation rapidly spreading in the monolayer. In addition, $Na_V1.8$, one of the prominent subtypes present in hESC-RPE [4], has a comparatively depolarized half-inactivation potential of ~ −30 mV [42, 43]. If $Na_V1.8$ contributes to any substantial level, its big portion would be available for activation at rest. Thus, taking into account the presence of several types of voltage-gated ion channels in the RPE, intrinsic properties of RPE membrane and its hyperpolarization in the transition from dark to light, the capacity for spiking makes sense and supports the role of RPE as much more versatile tissue than merely giving homeostatic support to the retina.

Fluctuating membrane leak

Membrane conductance fluctuated in virtually all cells with current-clamp recordings. Similarly, in the voltage clamp experiments, changes in leak occurring in the course of seconds were also observed routinely. The finding of a large, spontaneously and rapidly fluctuating depolarizing conductance is unusual. However, the crucial question is whether the observed changes in R_m reflect genuine, ion channel-dependent changes in membrane conductance, or are due to seal instability. Although this problem cannot be solved decisively without additional pharmacological/genetic studies of ion channels that could mediate leak conductance(s), there are several arguments in support of the physiological leak hypothesis. Changes in leak conductance in the range from 10 to about 0.5 nS localized at the membrane-electrode interface in the whole-cell configuration usually cause irreversible seal disruption. A non-selective instrumental conductance caused by imperfect attachment of plasma membrane to the electrode glass would dissipate the local transmembrane ionic gradients in the vicinity of the membrane-electrode interface. This would immediately diminish the recorded voltage-activated ionic currents as is observed with bad seals, and lead to quick run-down. Our experience with other types of cells suggests that although seal quality can slowly improve over

Ignatova *et al. BMC Biology*   (2023) 21:84

Page 15 of 19

time, especially in the beginning of an experiment, and thus increase whole-cell resistance, the opposite leak-increasing changes quickly ruin the experiment. Continuous and rapid fluctuations of leak occurring repeatedly over the course of many minutes are inconsistent with the seal instability hypothesis.

Assuming that the fluctuating leak was physiological, what channels could mediate it? The leak current is overall depolarizing, indicating that K^+ channels in the plasma membrane cannot dominate it above the K^+ reversal potential of -90 mV. However, although membrane properties appeared to be passive both in high- and low-resistance states (Figs. 3B, E and 8F) suggesting that leak channels are not voltage-activated, changes in leak appear to be associated with strong changes in membrane potential (Figs. 7A, D and 8G–K). Thus, it is possible that when membrane is strongly hyperpolarized by a current pulse, voltage-dependent inward rectifier K^+ channels [44, 45] open and provide rapid depolarization, contributing to the sharp depolarizing transients we observed (Fig. 9). However, these channels tend to close with depolarization (Fig. 1E). At membrane potentials more negative than the reversal potential for Cl^- (-39 mV in our experiments), efflux of Cl^- via various chloride channels [6, 8] could mediate a depolarizing leak current.

However, we argue that leak current fluctuations are probably caused by changes in gap junction conductance [46, 47]. Under physiological conditions, RPE cells face three external ionic milieus, two on the apical and basal surfaces and that/those of the neighboring cells. In our experiments, the trans-epithelial chemical gradient was disrupted but the intercellular ionic gradient probably exacerbated after the cytosol equilibrated with the patch pipette solution. RPE cells express Cx43-based gap junctions [11, 17, 48] that have voltage-dependent gating properties [47], so a strong depolarization or hyperpolarization of the clamped cell can change the transjunctional potential, leading to the opening or closing of gap junctions. This is consistent with the observation that sudden changes in leak were associated with strong changes in membrane potential during current-clamp experiments (Fig. 7A, D). Furthermore, recent studies reveal the presence of functional Cx43 hemichannels largely on the apical membrane of human and mouse RPE [11, 17]. Opening or closing of Cx43 hemichannels expressed in the plasma membrane could contribute to the changes in R_m observed in this work.

Spread of electrical excitation in RPE

Delayed activation of sodium currents characterized by more positive reversal potential than that of the normal I_{Na} is often observed in neurons with elongated branches. The so-called escaping currents are caused by inadequate space clamp [49, 50]. In the small hexagonally shaped RPE cells, however, I_{Na} can escape not from a distal dendrite or axon but from the neighboring cells connected with open gap junctions.

Gap junctional coupling between cells in the RPE monolayer is likely to promote synchronization of various processes, and its role in eye development has been shown in the developing chick [48, 51]. While it is known that gap junctions in RPE allow the spread of electrical signals [17, 52], here we demonstrated evidence that electrical coupling could be strong enough to allow spread of I_{Na}-mediated excitation waves to the neighbors of the patched cell (Fig. 10C, F).

We propose the following mechanism for the generation of the delayed inward currents observed in this study. When the patched cell is connected to its neighbors via open gap junctions, they introduce additional junctional resistance (R_{GJ}) in series with the electrode series resistance (R_s), so that charging of the neighboring cell is governed by the sum of two series resistances and its R_m, and the higher the ratio of $R_{GJ} + R_s$ to the second cell's R_m, the smaller the voltage drop on the membrane. Consequently, the neighboring cells can be clamped via gap junctions but the eventual membrane voltage and the speed of its change will depend on $R_{GJ} + R_s$. When R_{GJ} is relatively small, the clamping of the second cell, while accomplished with probably tens of mV voltage errors, could still yield enough I_{Na} to be detected across the junction. Conversely, when R_{GJ} is large, the other cell's voltage cannot be commanded to a degree sufficient to either recover I_{Na} or reach its activation threshold. Thus, multiple delayed currents probably arise in different neighboring cells with dissimilar but permissive R_{GJ} values, and if R_{GJ} values of two or more connections are about the same, their delayed currents would merge. Similar but comparatively slow processes can occur during current injections in the current-clamp experiments.

It is even possible that if R_{GJ} is very low, providing large conductance, the delayed current can merge with the primary I_{Na}. If R_{GJ} can indeed fluctuate dynamically then this might explain the broadening of I_{Na} in Fig. 10H right sub-panel compared to the left sub-panel. However, such cells would still be characterized by slow settling of the capacitance transient in the voltage clamp indicative of clamping across the junctions.

It appears that in the absolute majority of RPE cells the R_{GJ} was too high to enable delayed inward currents. This is supported by our experiments with Cx43 inhibitor 18α-GA, which resulted in a significant but comparatively small effect on membrane capacitance (Fig. 11F). While the cause of observed variability in gap junctional conductance is not clear, in addition to the transjunctional potential, gap junctions are regulated by many

Ignatova *et al. BMC Biology*   (2023) 21:84

Page 16 of 19

mechanisms, including internal Ca^{2+} concentration, elevation of which can rapidly and completely close the gap junction channels [35, 53, 54]. It was reported that increase of the cytosolic Ca^{2+} concentration after application of the calcium ionophore ionomycin resulted in a reduction of Cx43 gap junction conductance by a chemical gating mechanism [53]. In RPE, calcium can enter the cell from the extracellular space via TRP and L-type Ca^{2+} channels, from the endoplasmic reticulum via IP_3R channels, and from the neighboring cells via gap junctions [6, 51], and these sources might manifest dissimilarly in different cells.

It is possible that in the cells where delayed inward currents were observed, L-type Ca^{2+} channels could be the main source of Ca^{2+} influx. When voltage in such cells is held below the L-type Ca^{2+} channel activation threshold, either by clamping membrane potential to −80 mV in the voltage clamp, or by injecting a hyperpolarizing current in the current clamp, the influx of Ca^{2+} would be minimized and the gap junction blockade relieved. However, when the cell is depolarized during the test pulses, inward Ca^{2+} current would resume, partly blocking the gap junction channels. Then, as nifedipine blocked the L-type Ca^{2+} channels, Ca^{2+} influx stopped even during the depolarizations, thus maximizing the gap junction conductance, and increasing the delayed inward current amplitude and speeding up its onset (Fig. 11). Alternatively, cells characterized by the delayed inward currents could express more gap junction channels so that the same fraction of gap junction conductance as in the "normal" cells would produce sufficiently low R_{GJ} to elicit I_{Na}. Finally, it is worth keeping in mind that Cx43 gap junctions are suggested to be involved in ephaptic coupling, e.g., in vertebrate retina [55] and heart [56], strengthening the spread of depolarization to the nearby cells. We have previously shown that in RPE, both gap junctions and voltage-gated Na^+ channels localize to the tight junctions between the cells [4, 17] generating conditions where neighboring cell membranes containing these channels are closely associated. This could support ephaptic coupling eliciting an intriguing aspect for future studies.

Conclusions

The present work reveals how non-neuronal RPE cells residing in vivo in the immediate interactive contact with neuronal retina have active intrinsic properties. Remarkably, these cells can change the properties not only as response to the relatively slow changes in the ionic milieu associated with illumination-dependent changes in photoreceptor functioning, but also rapidly, on the scale of seconds, influence the electrophysiological states of the neighboring cells. Our studies demonstrate that in RPE, currents through Na^+ channels mediate voltage spikes

that can spread laterally in the monolayer through gap junctions. In addition, membrane resistance in the RPE shows immense and spontaneous fluctuations causing correlated alterations in the membrane potential. These properties enable mutual and previously uncovered interaction between RPE and the neural retina yet requiring further investigation with undisturbed physical interaction between the two tissues.

Methods

Cell culture

Two previously derived hESC lines Regea08/017 and Regea11/013 were used in this study. These lines have been established from the blastocyst-stage human embryos using mechanical derivation methods [57]. The hESC lines were cultured and differentiated into RPE as previously described [58, 59] followed by cryopreservation [28, 60]. The cells were plated on hanging cell culture inserts (polyethylene terephthalate membrane with 1.0 μm pore size, Sarstedt, Inc., Newton, NC, USA) coated with Biolaminin LN 521 (1.8 μg/cm^2) and Collagen IV (10 μg/cm^2) with a density of 5.5×10^5 cells/cm^2. Inserts were placed in 24-well plates (Corning Inc., Corning, NY, USA) and cell monolayers nourished from both the apical and basolateral sides. For our experiments, the cells were cultured at +37 °C in 5% CO_2 in Knock-Out Dulbecco's modified Eagle's medium (KO-DMEM) containing 15% Knock-Out serum replacement (KO-SR), 1% Glutamax, 0.2% 2-mercaptoethanol (all from Thermo Fisher Scientific, Waltham, MA, USA), 1% non-essential amino acids (NEAA), and 50 U/mL penicillin/streptomycin (both from Lonza Group, Basel, Switzerland). The medium was replenished three times a week.

Patch-clamp recordings

Cells cultured for 4–26 weeks from several independent differentiation batches were used. Current and voltage recordings were obtained from hESC-RPE monolayers using the standard patch-clamp technique in the whole-cell configuration. Patch-clamp pipettes were pulled from borosilicate glass capillaries (0.86 mm I.D. 1.5 mm O.D., Science Products GmbH, Hofheim, Germany and Harvard apparatus, Holliston, MA, USA) using a filament-based puller P-1000 (Sutter Instrument, Novato, CA, USA). Pipettes were filled with an internal solution containing (in mM): 83 K-gluconate, 25 KCl, 5.5 EGTA, 0.5 $CaCl_2$, 4 ATP-Mg, 0.1 GTP-Na, 10 HEPES, and 5 NaCl (pH adjusted to 7.2 with KOH and osmolarity to 290 mOsm with sucrose). The final electrode resistance was between 4 and 7 MΩ. In some experiments (Fig. 11F–K and Additional file 1. Fig. S1), K-gluconate (83 mM) and KCl (25 mM) in the pipette solution were replaced with $CsCH_3SO_3$ (83 mM) and CsCl (25 mM).

RPE monolayers were continuously superfused with Ames' solution (Sigma-Aldrich, St. Louis, MO, USA) supplemented with 10 mM HEPES and 10 mM NaCl (pH adjusted to 7.4 with NaOH and osmolarity to 315 mOsm with sucrose).

Extracellular solution was heated to 33–35 °C with the inline heater SH-27B controlled with a TC-324B unit (Warner Instruments, Hamden, CT, USA). In some experiments, nifedipine or 18α-glycyrrhetinic acid (both 10 μM, Sigma-Aldrich, St. Louis, MO, USA), or TTX citrate (10 μM, Abcam, Cambridge, UK) was added to the bath solutions.

All recordings were made using Axopatch 200B patch-clamp amplifier connected to Digidata 1440A converter (Molecular Devices, San Jose, CA, USA). Currents were recorded at the sampling frequency of 250 kHz and low-pass filtered at 2 kHz. Holding potential was −70 mV in all voltage clamp experiments. Resting membrane potential (V_{rest}) was determined from the current clamp in the absence of current injection. Only recordings with series resistance of ≤ 25 MΩ were used. Liquid junction potential calculated according to the Nernst-Planck equation was +13 mV. Data presented in the text and figures were not compensated for the liquid junction potential. Capacitance compensation was used to full extent. In the majority of cells, series resistance was compensated by the built-in circuit of the amplifier (20–80% correction).

Equilibrium potentials calculated from the patch pipette and bath solutions concentrations were −90.1 mV for E_K, 85.8 mV for E_{Na}, 221.7 mV for E_{Ca}, and −39.3 mV for E_{Cl}.

Data analysis and statistics

The character of data distribution was measured using the Shapiro-Wilk normality test. Data in the samples that generally did not pass the normality test are presented in the text as medians with 1st:3rd interquartile ranges. In pairwise comparisons, such data were statistically compared using Mann–Whitney *U*-test (MWUT). All normally distributed cumulative data were presented as means ± standard deviation (s.d.). Significance testing was performed using the *t*-test as indicated. Pearson's correlation coefficient (*r*) was used for the analyses of correlations. Throughout the text, (*n*) denotes the group size.

Abbreviations

C_m	Membrane capacitance
g	Conductance
hESC-RPE	Human embryonic stem cell-derived retinal pigment epithelium
I_C	Capacitive current
I_{IR}	Sustained hyperpolarization-activated inward current
I_{Na}	Voltage-activated Na$^+$ current
I_K	Voltage-activated K$^+$ current
I_A	Transient outward voltage-activated K$^+$ current
I_{DR}	Sustained voltage-activated K$^+$ current
POS	Photoreceptor outer segments
R_m	Membrane resistance
R_{GJ}	Junctional resistance
R_s	Series resistance
SSI	Steady-state inactivation
TTX	Tetrodotoxin
V_{rest}	Resting potential
τ_m	Membrane time constant
τ_{rec}	Recovery time constant
18α-GA	18α-glycyrrhetinic acid

Supplementary Information

The online version contains supplementary material available at https://doi.org/10.1186/s12915-023-01559-5.

Additional file 1: Fig. S1. Kinetics of I_{Na} recorded using cesium-based intracellular solution

Additional file 2: Table S1. Datasets

Availability of data and materials

All data generated or analyzed during this study are included in this published article, its supplementary information files (Additional file 1: Fig. S1, Additional file 2: Table S1), and Figshare data repository [61]. Where *n* < 6, the individual data values are provided in additional files (Additional file 2: Table S1) and cited in the figure legends.

Declarations

Ethics approval and consent to participate

Tampere University has approval (Dnro 1426/32/300/05) from the National Supervisory Authority for Welfare and Health, Finland, for the research with human embryos. The local Ethical Committee of the Pirkanmaa Hospital District, Finland, has granted a supportive statement to derive, expand, and differentiate hESC lines from surplus embryos for research purposes (R05116). No new cell lines have been derived in this study.

Consent for publication

Not applicable.

Competing interests

The authors declare that they have no competing interests.

Ignatova *et al. BMC Biology*   (2023) 21:84

Page 18 of 19

References

1. Sparrow JR, Hicks D, Hamel CP. The retinal pigment epithelium in health and disease. Curr Mol Med. 2010;10(9):802–23.
2. Strauss O. The retinal pigment epithelium in visual function. Physiol Rev. 2005;85(3):845–81.
3. Giblin JP, Comes N, Strauss O, Gasull X. Ion channels in the eye: involvement in ocular pathologies. Adv Protein Chem Struct Biol. 2016;104:157–231.
4. Johansson JK, Karema-Jokinen VI, Hakanen S, Jylhä A, Uusitalo H, Vihinen-Ranta M, et al. Sodium channels enable fast electrical signaling and regulate phagocytosis in the retinal pigment epithelium. BMC Biology. 2019;17(1):63.
5. Korkka I, Viheriala T, Juuti-Uusitalo K, Uusitalo-Jarvinen H, Skottman H, Hyttinen J, et al. Functional voltage-gated calcium channels are present in human embryonic stem cell-derived retinal pigment epithelium. Stem Cells Transl Med. 2019;8(2):179–93.
6. Wimmers S, Karl MO, Strauss O. Ion channels in the RPE. Prog Retin Eye Res. 2007;26(3):263–301.
7. Hughes BA, Takahira M, Segawa Y. An outwardly rectifying K+ current active near resting potential in human retinal pigment epithelial cells. Am J Physiol. 1995;269(1 Pt 1):C179-87.
8. Reichhart N, Strauss O. Ion channels and transporters of the retinal pigment epithelium. Exp Eye Res. 2014;126:27–37.
9. Strauss O. Transport mechanisms of the retinal pigment epithelium to maintain of visual function. Heat and Mass Transfer. 2014;50(3):303–13.
10. Rosenthal R, Heimann H, Agostini H, Martin G, Hansen LL, Strauss O. Ca2+ channels in retinal pigment epithelial cells regulate vascular endothelial growth factor secretion rates in health and disease. Mol Vis. 2007;13:443–56.
11. Akanuma SI, Higashi H, Maruyama S, Murakami K, Tachikawa M, Kubo Y, et al. Expression and function of connexin 43 protein in mouse and human retinal pigment epithelial cells as hemichannels and gap junction proteins. Exp Eye Res. 2018;168:128–37.
12. Wen R, Lui GM, Steinberg RH. Whole-cell K+ currents in fresh and cultured cells of the human and monkey retinal pigment epithelium. J Physiol. 1993;465:121–47.
13. Wen R, Lui GM, Steinberg RH. Expression of a tetrodotoxin-sensitive Na+ current in cultured human retinal pigment epithelial cells. J Physiol. 1994;476(2):187–96.
14. Sakai H, Saito T. Na+ and Ca2+ channel expression in cultured newt retinal pigment epithelial cells: comparison with neuronal types of ion channels. J Neurobiol. 1997;32(4):377–90.
15. Pattnaik BR, Hughes BA. Effects of KCNQ channel modulators on the M-type potassium current in primate retinal pigment epithelium. Am J Physiol Cell Physiol. 2012;302(5):C821-33.
16. Botchkin LM, Matthews G. Voltage-dependent sodium channels develop in rat retinal pigment epithelium cells in culture. Proc Natl Acad Sci U S A. 1994;91(10):4564–8.
17. Fadjukov J, Wienbar S, Hakanen S, Aho V, Vihinen-Ranta M, Ihalainen TO, et al. Gap junctions and connexin hemichannels both contribute to the electrical properties of retinal pigment epithelium. J Gen Physiol. 2022;154(4):202112916.
18. Korkka I, Skottman H, Nymark S. Heterogeneity of potassium channels in human embryonic stem cell-derived retinal pigment epithelium. Stem Cells Transl Med. 2022;11(7):753–66.
19. Sakai H, Saito T. Development of voltage-dependent inward currents in dissociated newt retinal pigment epithelial cells in culture. Neuroreport. 1994;5(8):933–6.
20. Barres BA, Chun LL, Corey DP. Ion channel expression by white matter glia: I. type 2 astrocytes and oligodendrocytes. Glia. 1988;1(1):10–30.
21. Sontheimer H, Black JA, Ransom BR, Waxman SG. Ion channels in spinal cord astrocytes in vitro. I. transient expression of high levels of Na+ and K+ channels. J Neurophysiol. 1992;68(4):985–1000.
22. Sontheimer H, Waxman SG. Ion channels in spinal cord astrocytes in vitro. II. biophysical and pharmacological analysis of two Na+ current types. J Neurophysiol. 1992;68(4):1001–11.
23. Fain GL, Farahbakhsh NA. Voltage-activated currents recorded from rabbit pigmented ciliary body epithelial cells in culture. J Physiol. 1989;418:83–103.
24. Forest DL, Johnson LV, Clegg DO. Cellular models and therapies for age-related macular degeneration. Dis Model Mech. 2015;8(5):421–7.
25. Schwartz SD, Regillo CD, Lam BL, Eliott D, Rosenfeld PJ, Gregori NZ, et al. Human embryonic stem cell-derived retinal pigment epithelium in patients with age-related macular degeneration and Stargardt's macular dystrophy: follow-up of two open-label phase 1/2 studies. Lancet. 2015;385(9967):509–16.
26. Sharma R, Bose D, Maminishkis A, Bharti K. Retinal pigment epithelium replacement therapy for age-related macular degeneration: are we there yet? Annu Rev Pharmacol Toxicol. 2020;60:553–72.
27. Limnios IJ, Chau YQ, Skabo SJ, Surrao DC, O'Neill HC. Efficient differentiation of human embryonic stem cells to retinal pigment epithelium under defined conditions. Stem Cell Res Ther. 2021;12(1):248.
28. Hongisto H, Jylha A, Nattinen J, Rieck J, Ilmarinen T, Vereb Z, et al. Comparative proteomic analysis of human embryonic stem cell-derived and primary human retinal pigment epithelium. Sci Rep. 2017;7(1):6016.
29. Carr AJ, Smart MJ, Ramsden CM, Powner MB, da Cruz L, Coffey PJ. Development of human embryonic stem cell therapies for age-related macular degeneration. Trends Neurosci. 2013;36(7):385–95.
30. Sorkio A, Hongisto H, Kaarniranta K, Uusitalo H, Juuti-Uusitalo K, Skottman H. Structure and barrier properties of human embryonic stem cell-derived retinal pigment epithelial cells are affected by extracellular matrix protein coating. Tissue Eng Part A. 2014;20(3–4):622–34.
31. Burgess DE, Crawford O, Delisle BP, Satin J. Mechanism of inactivation gating of human T-type (low-voltage activated) calcium channels. Biophys J. 2002;82(4):1894–906.
32. Hille B. Ion Channels of Excitable Membranes. 3rd ed. Sunderland, MA: Sinauer Associates; 2001.
33. Goldman L. Internal cesium and the sodium inactivation gate in Myxicola giant axons. Biophys J. 1986;50(2):231–8.
34. Ignatova II, French AS, Torkkeli PH, Liu H, Frolov RV. Suppression of Gq and PLC gene expression has a small effect on quantum bumps in vivo in Periplaneta americana. J Comp Physiol A Neuroethol Sens Neural Behav Physiol. 2020;206(4):597–610.
35. Peracchia C. Calmodulin-mediated regulation of gap junction channels. Int J Mol Sci. 2020;21(2):485.
36. Guo Y, Martinez-Williams C, Gilbert KA, Rannels DE. Inhibition of gap junction communication in alveolar epithelial cells by 18alpha-glycyrrhetinic acid. Am J Physiol. 1999;276(6):L1018-26.
37. Roden DM, Balser JR, George AL Jr, Anderson ME. Cardiac ion channels. Annu Rev Physiol. 2002;64:431–75.
38. Prajapati C, Polonen RP, Aalto-Setala K. Simultaneous recordings of action potentials and calcium transients from human induced pluripotent stem cell derived cardiomyocytes. Biol Open. 2018;7(7):035030.
39. Lakkaraju A, Umapathy A, Tan LX, Daniele L, Philp NJ, Boesze-Battaglia K, et al. The cell biology of the retinal pigment epithelium. Prog Retin Eye Res. 2020:100846.
40. Karl MO, Kroeger W, Wimmers S, Milenkovic VM, Valtink M, Engelmann K, et al. Endogenous Gas6 and Ca2+ -channel activation modulate phagocytosis by retinal pigment epithelium. Cell Signal. 2008;20(6):1159–68.
41. Muller C, Mas Gomez N, Ruth P, Strauss O. CaV1.3 L-type channels, maxiK Ca(2+)-dependent K(+) channels and bestrophin-1 regulate rhythmic photoreceptor outer segment phagocytosis by retinal pigment epithelial cells. Cell Signal. 2014;26(5):968–78.
42. Akopian AN, Sivilotti L, Wood JN. A tetrodotoxin-resistant voltage-gated sodium channel expressed by sensory neurons. Nature. 1996;379(6562):257–62.
43. Han C, Vasylyev D, Macala LJ, Gerrits MM, Hoeijmakers JG, Bekelaar KJ, et al. The G1662S NaV1.8 mutation in small fibre neuropathy: impaired inactivation underlying DRG neuron hyperexcitability. J Neurol Neurosurg Psychiatry. 2014;85(5):499–505.
44. Huang H, Li H, Shi K, Wang L, Zhang X, Zhu X. TREKTRAAK twopore domain potassium channels protect human retinal pigment epithelium cells from oxidative stress. Int J Mol Med. 2018;42(5):2584–94.
45. Shen C, Ma W, Zheng W, Huang H, Xia R, Li C, et al. The antioxidant effects of riluzole on the APRE-19 celll model injury-induced by t-BHP. BMC Ophthalmol. 2017;17(1):210.
46. Bukauskas FF, Verselis VK. Gap junction channel gating. Biochim Biophys Acta. 2004;1662(1–2):42–60.
47. Gonzalez D, Gomez-Hernandez JM, Barrio LC. Molecular basis of voltage dependence of connexin channels: an integrative appraisal. Prog Biophys Mol Biol. 2007;94(1–2):66–106.

48. Pearson RA, Dale N, Llaudet E, Mobbs P. ATP released via gap junction hemichannels from the pigment epithelium regulates neural retinal progenitor proliferation. Neuron. 2005;46(5):731–44.
49. Sontheimer H, Ransom CB. Whole-cell patch-clamp recordings. In: Walz W, Boulton AA, Baker GB, editors. Patch-clamp analysis: advanced techniques. Totowa, NJ: Humana Press; 2002. p. 35–67.
50. Milescu LS, Bean BP, Smith JC. Isolation of somatic Na+ currents by selective inactivation of axonal channels with a voltage prepulse. J Neurosci. 2010;30(22):7740–8.
51. Pearson RA, Catsicas M, Becker DL, Bayley P, Luneborg NL, Mobbs P. Ca(2+) signalling and gap junction coupling within and between pigment epithelium and neural retina in the developing chick. Eur J Neurosci. 2004;19(9):2435–45.
52. Hudspeth AJ, Yee AG. The intercellular junctional complexes of retinal pigment epithelia. Invest Ophthalmol. 1973;12(5):354–65.
53. Xu Q, Kopp RF, Chen Y, Yang JJ, Roe MW, Veenstra RD. Gating of connexin 43 gap junctions by a cytoplasmic loop calmodulin binding domain. Am J Physiol Cell Physiol. 2012;302(10):C1548-56.
54. Bennett BC, Purdy MD, Baker KA, Acharya C, McIntire WE, Stevens RC, et al. An electrostatic mechanism for Ca(2+)-mediated regulation of gap junction channels. Nat Commun. 2016;7:8770.
55. Vroman R, Klaassen LJ, Kamermans M. Ephaptic communication in the vertebrate retina. Front Hum Neurosci. 2013;7:612.
56. Veeraraghavan R, Hoeker GS, Alvarez-Laviada A, Hoagland D, Wan X, King DR, et al. The adhesion function of the sodium channel beta subunit (β1) contributes to cardiac action potential propagation. eLife. 2018;7:e37610.
57. Skottman H. Derivation and characterization of three new human embryonic stem cell lines in Finland. In Vitro Cell Dev Biol Anim. 2010;46(3–4):206–9.
58. Vaajasaari H, Ilmarinen T, Juuti-Uusitalo K, Rajala K, Onnela N, Narkilahti S, et al. Toward the defined and xeno-free differentiation of functional human pluripotent stem cell-derived retinal pigment epithelial cells. Mol Vis. 2011;17:558–75.
59. Skottman H, Muranen J, Lahdekorpi H, Pajula E, Makela K, Koivusalo L, et al. Contacting co-culture of human retinal microvascular endothelial cells alters barrier function of human embryonic stem cell derived retinal pigment epithelial cells. Exp Cell Res. 2017;359(1):101–11.
60. Hongisto H, Ilmarinen T, Vattulainen M, Mikhailova A, Skottman H. Xeno- and feeder-free differentiation of human pluripotent stem cells to two distinct ocular epithelial cell types using simple modifications of one method. Stem Cell Res Ther. 2017;8(1):291.
61. Ignatova I, Frolov R, Nymark S. Electrical excitability and its lateral spread in the retinal pigment epithelium: dataset. 2023. https://doi.org/10.6084/m9.figshare.22246969.v2.

Publisher's Note

Springer Nature remains neutral with regard to jurisdictional claims in published maps and institutional affiliations.